

## Prospects for fast Rydberg gates on an atom chip

Matthias M. Müller · Harald R. Haakh ·  
Tommaso Calarco · Christiane P. Koch ·  
Carsten Henkel

Received: date / Accepted: date

**Abstract** Atom chips are a promising candidate for a scalable architecture for quantum information processing provided a universal set of gates can be implemented with high fidelity. The difficult part in achieving universality is the entangling two-qubit gate. We consider a Rydberg phase gate for two atoms trapped on a chip and employ optimal control theory to find the shortest gate that still yields a reasonable gate error. Our parameters correspond to a situation where the Rydberg blockade regime is not yet reached. We discuss the role of spontaneous emission and the effect of noise from the chip surface on the atoms in the Rydberg state.

**Keywords** Optimal control · phase gate · Rydberg atoms · cavity quantum electrodynamics

### 1 Introduction

Neutral trapped atoms allow for qubit encoding in metastable internal states; they offer long decoherence times and can easily be controlled by optical and magnetic fields. This makes them a promising candidate for the realization of a quantum computer [1]. Since the atoms hardly interact with each other, the largest difficulty encountered when building such a quantum computer is the implementation of an entangling two-qubit operation. The clock speed is thus typically limited by the gate operation time for one two-qubit gate which, together with several single-qubit operations, provides universal quantum computing [2].

---

Matthias M. Müller, Tommaso Calarco  
Institut für Quanteninformationsverarbeitung, Universität Ulm, 89081 Ulm, Germany

Harald R. Haakh, Carsten Henkel  
Institut für Physik und Astronomie, Universität Potsdam, Karl-Liebknecht-Str. 24/25, 14476  
Potsdam, Germany

Christiane P. Koch  
Institut für Physik, Universität Kassel, Heinrich-Plett-Str. 40, 34132 Kassel, Germany  
E-mail: christiane.koch@uni-kassel.de

A number of schemes to entangle qubits carried by neutral atoms have been proposed [3, 4, 5, 6, 7, 8, 9, 10, 11]. An estimate of the corresponding gate duration is obtained in terms of the inverse of the interaction strength promoting the entanglement. Adiabatic time evolution is not essential; it can be avoided by employing optimal control theory [12, 13, 14, 15, 16]. In fact, optimal control theory is an extremely versatile tool that allows for achieving a high-fidelity implementation of desired quantum tasks. Moreover, it can be used to determine what fundamentally limits fidelity and duration of a quantum operation [17].

For a two-qubit gate with neutral atoms, the highest gate speeds can be expected when the atoms are internally excited to expose them to long-range interactions, a prominent example being dipole-dipole forces between Rydberg atoms [6, 18, 19, 20]. However, care needs to be taken if the atoms are *resonantly* excited into a state with long-range interactions. For the example of the Rydberg gate, this will happen, e.g., if a perfectly entangling gate is desired but the distance between the atoms is too large to reach the Rydberg blockade regime [21]. The forces that induce entanglement will then couple internal electronic and vibrational dynamics, and the motional state of the atoms will have changed after the gate operation, implying strong leakage out of the quantum register. In principle, the vibrational excitation energy can be absorbed by an external field determined for example by optimal control theory. However, this requires the gate duration to be long enough to resolve the motional energy levels [22]. For resonant excitation into states with long-range interaction, the minimum duration, or quantum speed limit, for an entangling gate is thus limited either by the inverse interaction strength or by the vibrational period of the trap, whichever one is longer [21, 22].

Trapping, controlling and entangling two atoms is just the very first step towards a neutral atom based quantum computer. A scalable architecture is required to assemble many qubits and carry out any meaningful computation. One possibility to achieve scalability is given by miniaturizing the tools for trapping and manipulating the atoms to fit on a micrometer-sized chip [23, 24, 25]. These microtraps offer strong confinement (fast vibrational motion) that may help in fast entangling gates. However, the close proximity of the atoms to the surface of the chip introduces noise sources which might significantly compromise the gate performance. Here, we study whether the fastest possible entangling gates for neutral atoms known to date – optimal Rydberg phase gates at the quantum speed limit – can be implemented on an atom chip, despite the presence of noise. To this end, we present an optimal control analysis for a pulsed excitation scheme of two atoms, using trap parameters realistic for microtraps. The analysis includes the nuclear motion of the atom pair and addresses the influence of spontaneous emission from electronically excited states. We also estimate the influence of electric fields (static and dynamic) that arise from surface contamination and from blackbody and thermal near field radiation. Attention is paid to the specific properties of the fragile, highly excited Rydberg states that show huge electric dipole moments. Our results suggest that a fast gate (on the scale of some 10 ns) is possible with errors on the level of  $10^{-3}$ . We identify options for reducing this error by another order of magnitude to reach the fault tolerance threshold.

## 2 Fast phase gates via optimal control

### 2.1 Controlled phase gate via Rydberg interaction of neutral atoms

We consider two rubidium atoms that are trapped with a typical distance of  $4\ \mu\text{m}$  between them. The atoms sit in the ground state of the trap which is assumed to be deep enough such that each well can be approximated by a harmonic potential. The qubit states are encoded in two hyperfine levels of the ground state, for example  $|0\rangle = |5s_{1/2}, F=2, M_F=2\rangle$ ,  $|1\rangle = |5s_{1/2}, F=1, M_F=1\rangle$ . A controlled phase gate can be implemented by excitation to a Rydberg state where the two atoms are exposed to a long-range interaction [6]. In a recent experiment with two rubidium atoms held in optical tweezers [26], the  $|r\rangle = |5d_{3/2}, F=3, M_F=3\rangle$  Rydberg state was accessed by a near-resonant two-photon transition via the  $|i\rangle = |5p_{1/2}, F=2, M_F=2\rangle$  intermediate state. The Hamiltonian for a single trapped atom in the rotating-wave approximation reads

$$\begin{aligned} \hat{\mathbf{H}}^{(1)}(t) = & \sum_{j=0,1} |j\rangle\langle j| \otimes \left( \hat{\mathbf{T}}_{\hat{\mathbf{r}}} + V_{trap}^j(\hat{\mathbf{r}}) \right) \\ & + |i\rangle\langle i| \otimes \left( \hat{\mathbf{T}}_{\hat{\mathbf{r}}} + V_{trap}^i(\hat{\mathbf{r}}) + \frac{\Delta}{2} \right) + |r\rangle\langle r| \otimes \left( \hat{\mathbf{T}}_{\hat{\mathbf{r}}} + V_{trap}^r(\hat{\mathbf{r}}) + \frac{\delta}{2} \right) \\ & + \frac{\Omega_R(t)}{2} \left( |0\rangle\langle i| + |i\rangle\langle 0| \right) \otimes \mathbb{1}(\hat{\mathbf{r}}) + \frac{\Omega_B(t)}{2} \left( |i\rangle\langle r| + |r\rangle\langle i| \right) \otimes \mathbb{1}(\hat{\mathbf{r}}). \end{aligned} \quad (1)$$

Here,  $\hat{\mathbf{r}}$  denotes the position operator of the atom,  $\hat{\mathbf{T}}$  the kinetic energy operator, and  $\Omega_\lambda(t)$  ( $\lambda = R, B$ ) the time-dependent Rabi frequencies of the red and blue lasers (wavelengths 795 nm and 474 nm for the chosen Rydberg state). The Rabi frequencies are parametrized according to  $\Omega_\lambda(t) = \Omega_{j,0}(\tanh \varepsilon_\lambda(t) + 1)/2 \in [0, \Omega_{j,0}]$ , where  $\varepsilon_\lambda(t)$  will be determined by optimal control.  $\Delta$  denotes the detuning of the red laser with respect to the intermediate state. The two-photon detuning from the Rydberg level is given in terms of the Stark shift,  $\delta = (\Omega_{B,0}^2 - \Omega_{R,0}^2)/4\Delta$ . The corresponding level scheme is depicted in Fig. 1. The electronically excited states  $|i\rangle$  and  $|r\rangle$  decay via spontaneous emission, their lifetimes are 27.7 ns for  $|i\rangle$  and 210  $\mu\text{s}$  for  $|r\rangle$  (see also Sec. 3.3). The total Hamiltonian for the two atoms is given by

$$\hat{\mathbf{H}} = \hat{\mathbf{H}}_1^{(1)} \otimes \mathbb{1}_{4,2} \otimes \mathbb{1}_{\hat{\mathbf{r}}_2} + \mathbb{1}_{4,1} \otimes \mathbb{1}_{\hat{\mathbf{r}}_1} \otimes \hat{\mathbf{H}}_2^{(1)} + \hat{\mathbf{H}}_{int}^{(1,2)} \quad (2)$$

with the interaction term describing the long-range forces when both atoms are in the Rydberg state,

$$\hat{\mathbf{H}}_{int}^{(1,2)} = |rr\rangle\langle rr| \otimes \frac{c_3}{|\hat{\mathbf{r}}_1 - \hat{\mathbf{r}}_2|^3}. \quad (3)$$

The parameter  $c_3 = 3.433 \cdot 10^6$  a.u. = 3230 MHz  $\mu\text{m}^3$  has been calculated in Ref. [26] for the Rydberg levels  $|r\rangle$  and scales with the principal quantum number as  $n^4$  [20]. For an interatomic distance of  $r_0 = 4\ \mu\text{m}$  which is realistic for an experimental implementation, this yields an estimated interaction energy of 50 MHz. In all other states, the interaction between atoms that are thus far apart is so weak that it can be neglected. The harmonic approximation for the trapping potentials permits us to integrate over the center-of-mass motion of the two atoms and to focus on a one-dimensional model along the internuclear axis. We take an effective trap frequency  $\omega/2\pi \approx 276$  kHz (period 3.6  $\mu\text{s}$ ) for the interatomic distance coordinate

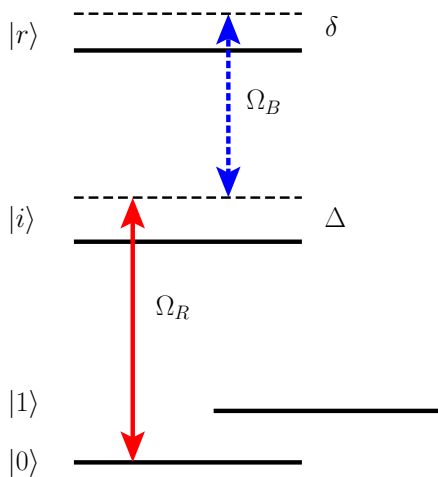


**Fig. 1** One-atom level scheme for near-resonant two-photon excitation to a Rydberg state.

$\hat{\mathbf{r}} = |\hat{\mathbf{r}}_1 - \hat{\mathbf{r}}_2|$  (ground state size  $\approx 20$  nm). This value is slightly larger than in the optical tweezer traps of Ref. [26], and may also be achieved in magnetic microtraps implemented on an atom chip [25]. The Hamiltonian, Eq. (2), is represented on an equidistant Fourier grid extending for  $\pm 0.3 \mu\text{m}$  around  $r_0 = 4 \mu\text{m}$ . The time evolution generated by this Hamiltonian is obtained by solving the time-dependent Schrödinger with the Chebychev propagator [27]. Note that we do not attempt here to spatially resolve the Rydberg orbits of the excited electron in the trapping fields. The level structure in a magnetic quadrupole field, for example, has been addressed in Refs. [28, 29].

## 2.2 Optimal control for two-qubit gates

Our goal is to implement the controlled phase gate on the qubit register basis  $\{|00\rangle, |01\rangle, |10\rangle, |11\rangle\}$ ,

$$\hat{\mathbf{O}} = \text{diag}(e^{i\chi}, 1, 1, 1) \quad \text{or} \quad \hat{\mathbf{O}} = \text{diag}(1, 1, 1, e^{i\chi}). \quad (4)$$

This can be achieved by finding suitable fields  $\varepsilon = \{\varepsilon_R(t), \varepsilon_B(t)\}$  that drive the system evolution from time zero to time  $T$  such that  $\hat{\mathbf{U}}(T, 0; \varepsilon) = \hat{\mathbf{O}}$  up to a global phase. The quality of the implementation is measured by the fidelity,  $F$ . A suitable choice for evaluating it is based on projecting the actual evolution  $\hat{\mathbf{U}}(T, 0; \varepsilon)$  onto the desired operation  $\hat{\mathbf{O}}$  [16],

$$F = \frac{1}{N} \left| \text{Tr} \left[ \hat{\mathbf{O}}^\dagger \hat{\mathbf{U}}(T, 0; \varepsilon) \right] \right|. \quad (5)$$

$N$  denotes the number of basis states,  $N = 4$  if  $\hat{\mathbf{O}}$  is a two-qubit gate. Note that the actual evolution can proceed in a Hilbert space which is much larger than the qubit register space. In our example, the dimension of the Hilbert space is  $4 \times 4 \times N_r$  where  $N_r$  is the number of grid points required to represent  $\hat{\mathbf{r}}$ . Then

$\hat{\mathbf{U}}(T, 0; \varepsilon)$  is obtained by a suitable projection onto the register space which in our example is spanned by  $|\varphi_0^{jj'}\rangle = |j\rangle \otimes |j'\rangle \otimes |\varphi_0\rangle$ ,  $j, j' = 0, 1$ , where  $|\varphi_0\rangle$  represents the ground state of the trap.

Optimal control treats the fidelity  $F$ ,  $F \in [0, 1]$ , as a functional of the control fields  $\varepsilon$ . Allowing for additional constraints such as minimization of the integrated pulse energy, leads to the total functional  $J$ ,

$$J = -F + \int_0^T g(\varepsilon) dt, \quad g(\varepsilon) = \frac{\alpha}{S(t)} [\varepsilon(t) - \varepsilon_{\text{ref}}(t)]^2, \quad (6)$$

which is to be minimized. Here  $\alpha$  is a weight,  $S(t)$  enforces the pulse to switch on and off smoothly, and  $\varepsilon_{\text{ref}}(t)$  is the control field at the previous optimization step. Variation of the functional  $J$  with respect to the evolving basis states and the control field yields a set of coupled optimization equations that are solved iteratively. We employ here a linear variant of Krotov's method in order to obtain a monotonically convergent optimization algorithm [16]. In particular, the update equation for the field is then given by

$$\Delta\varepsilon(t) = \varepsilon^{(k+1)}(t) - \varepsilon^{(k)}(t) = \frac{S(t)}{2\alpha} \sum_{jj'} \langle \varphi_0^{jj'} | \hat{\mathbf{O}}^+ \hat{\mathbf{U}}^+(t, T; \varepsilon^{(k)}) \hat{\boldsymbol{\mu}} \hat{\mathbf{U}}(t, 0; \varepsilon^{(k+1)}) | \varphi_0^{jj'} \rangle, \quad (7)$$

which matches at each time  $t$  the target states,  $\hat{\mathbf{O}}|\varphi_0^{jj'}\rangle$ , propagated backward in time under the old fields,  $\varepsilon^{(k)}$ , with the initial states, i.e., the basis states  $|\varphi_0^{jj'}\rangle$ , propagated forward in time under the new fields  $\varepsilon^{(k+1)}$ .

In our example of the Rydberg gate, the short lifetime of the intermediate state,  $|i\rangle$ , implies presence of a serious loss channel. The time evolution is then not unitary anymore. For dissipation due to spontaneous emission, the dynamics can be modeled by a Markovian Liouville-von Neumann equation for the density matrix with Lindblad dissipators. Optimal control theory can be adapted to such a situation [30, 31] but the numerical effort increases substantially. If dissipation is not needed to achieve the control objective but it rather represents a nuisance, a simpler approach is given by suppressing population in the dissipative channel. This is achieved by adding an additional constraint in the objective functional maximizing the expectation value of the projector onto the allowed subspace  $\hat{\mathbf{P}}_{\text{allow}} = (\mathbb{1} - |i\rangle\langle i|) \otimes (\mathbb{1} - |i\rangle\langle i|) \otimes \mathbb{1}_{\hat{r}}$ , i.e. the subspace of the total Hilbert space excluding the unstable state [32],

$$J = -F + \int_0^T g(\varepsilon) dt - \int_0^T \langle \hat{\mathbf{P}}_{\text{allow}} \rangle dt. \quad (8)$$

Provided the modified control objective is fulfilled, i.e., the dissipative channel is never populated, the dynamics can again be described by a Schrödinger equation. Including the state-dependent constraint does not modify the update equation for the field, Eq. (7), except for a source term in the equation for the backward propagation [32]. Such an inhomogeneous Schrödinger equation can be solved efficiently with a modified Chebychev propagator [33]. We test the success of this scheme by propagating the initial states under the optimal field, and adding the imaginary term  $-\frac{1}{2}\hbar\gamma_i|i\rangle\langle i|$  to the Hamiltonian (1), describing exponential decay from the intermediate state  $|i\rangle$ .

### 2.3 Limits for the duration of optimal gates

In the following, we employ the optimization algorithm with the standard functional (6) as well as with the functional (8) that minimizes the population in the unstable state. We are looking for the best compromise between high fidelity and fast operation.

The minimum gate durations are identified by running the optimization for varying  $T$ . If there is no loss, i.e., if we neglect spontaneous emission, our system is completely controllable. In the limit of sufficiently large  $T$ , the fidelity  $F$  then approaches one and the gate error approaches zero arbitrarily close [22]. As  $T$  is decreased, the time spent in the Rydberg state in which the atoms interact might become too short to pick up a non-local phase of  $\pi$  (time scale  $\pi\hbar r_0^3/c_3 \approx 10$  ns). This is the first and most obvious constraint that limits the gate time  $T$ . Secondly, when the atoms are in the Rydberg state (note that our interatomic distance is too large for the blockade regime to be reached, i.e., the atoms are resonantly excited into  $|rr\rangle$ ), they get accelerated in the attractive  $1/r^3$  potential. In principle, the optimization can find laser fields that absorb this vibrational energy. However, in order to find such laser fields, the algorithm needs to distinguish between the motional target state, the ground state of the trap, and higher excited states. The vibrational period of the trap ( $\approx 3.6 \mu\text{s}$ ) may therefore also limit the gate operation time. For shallow traps and a strong interaction, this second limit will be larger than the first one, and thus determine the minimum gate time  $T$  [22]. If the interaction  $c_3/r^3$  acts over a time such that a phase  $\pi$  is picked up, then a momentum of order  $\delta p = 3\pi\hbar/r_0$  is transferred to the relative motion. The motional error scales with the ratio to the momentum width in the ground state,  $(\hbar m\omega/4)^{1/2}$ , as  $1 - \exp[-\delta p^2/(2\hbar m\omega)] \approx \delta p^2/(2\hbar m\omega)$ , see also Ref. [8]. This translates into the condition that the ground state be much smaller than the mean distance,

$$\sqrt{\frac{\hbar}{m\omega}} \ll \frac{\sqrt{2}}{3\pi} r_0 \approx 0.15 r_0, \quad (9)$$

which is well met for our parameters since the trap ground state has a size  $\approx 20$  nm.

In our calculations the trap is only used to determine the initial state. During the action of the laser fields, the trapping potential is set to zero which corresponds to the dipole trap being switched off in the experiment [26]. We thus prevent the optimization algorithm from finding solutions that, if necessary, absorb vibrational energy. Once vibrational dynamics start to play a role, this will show up as a decrease in fidelity. However, this loss of fidelity could be avoided by leaving the trap on during the gate, in other words, it is not caused by a fundamental limit. Note that the trap is only needed to define the desired motional state at the end of the gate for the electronic ground state which carries the qubit state.

Finally, a third factor limiting the gate time  $T$  is due to spontaneous emission from the intermediate state. While it turns out that this limits the best possible fidelity in current implementations of the Rydberg gate [26], it is not a fundamental limit since one could think of accessing the Rydberg states differently, avoiding near-resonant two-photon excitation via such a strongly decaying state. We therefore discuss gate times and errors for both cases, including and neglecting spontaneous emission for the sake of comparison.

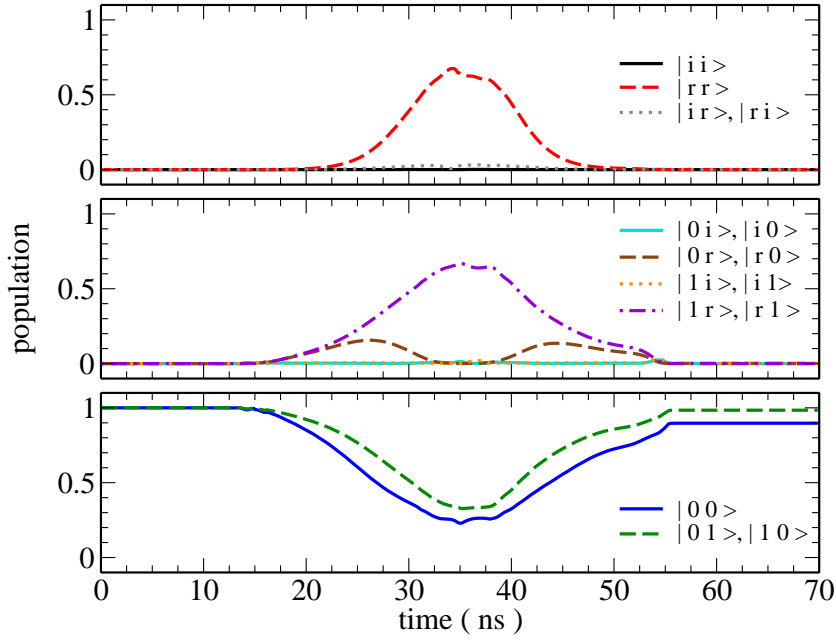
gate time $T$	gate error $\epsilon$	
	no loss	with loss
30ns	0.294	0.305
40ns	0.043	0.221
50ns	0.003	0.025
60ns	0.003	0.021
70ns	0.004	0.021
80ns	0.005	0.021

**Table 1** Optimal gate errors as a function of gate time. The optimization is performed here using the constraint that the population of the decaying intermediate state  $|i\rangle$  be minimized [control functional Eq.(8)]. The right column gives the gate error when the optimal pulse is applied and an exponential loss rate is assumed from the state  $|i\rangle$  (lifetime 27.7 ns).

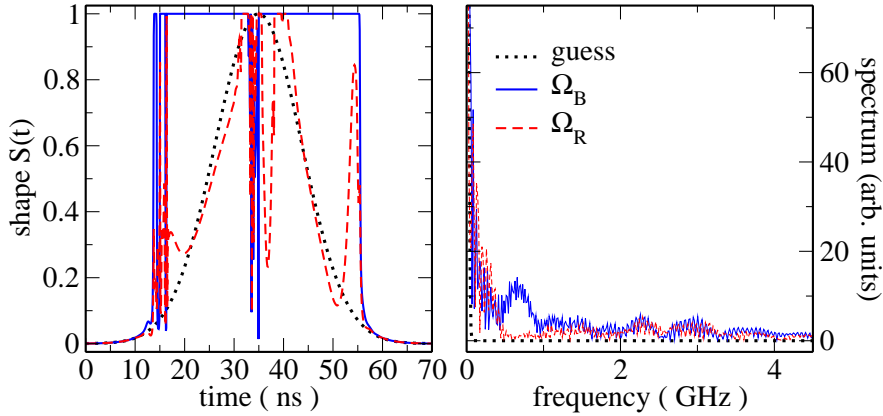
## 2.4 Minimizing spontaneous emission: adiabatic pulse sequence

Table 1 reports the minimal gate error  $\epsilon = 1 - F$  for a number of gate times  $T$ . Optimization was performed for a non-local phase in the  $|11\rangle$  state, utilizing the control functional (8), i.e., we avoid spontaneous decay by minimizing the population of the intermediate state,  $|i\rangle = |5p_{1/2}, F = 2, M_F = 2\rangle$ . Other noise sources are neglected yet (see estimates in Sec. 3 below). The calculation allows for maximum Rabi frequencies  $\Omega_{R,0} = \Omega_{B,0} = 2\pi \cdot 260$  MHz, cf. Ref. [26], and assumes a detuning  $\Delta = 2\pi \cdot 600$  MHz from  $|i\rangle$  (see Fig. 1). A number of  $N_r = 200$  spatial grid points is taken for the relative nuclear motion. For gate durations larger than 50 ns, gate errors of a few percent are obtained. The error increases only slightly when exponential loss from the state  $|i\rangle$  is taken into account (column “with loss”). The difference between the gate error with and without loss illustrates how well the condition of suppressing population in  $|i\rangle$  is fulfilled. For comparison, if the additional constraint is not employed in the optimization, the gate errors increase by two orders of magnitude to 20% and even more when spontaneous emission is taken into account. The gate errors without exponential decay in  $|i\rangle$  (central column of Table 1) illustrate when excitation of the motional degree of freedom start to play a role – for gate durations of 70 ns and larger, the error obtained without spontaneous emission is mainly due to excitation of higher trap states. Once spontaneous emission is included, this effect is, however, not dominant anymore.

The population dynamics of each electronic state induced by the optimal fields is shown in Fig. 2, demonstrating that indeed the intermediate state is almost never populated. The overall picture suggested by the population dynamics is an adiabatic transfer to and from the Rydberg state in a double-STIRAP-like fashion. This is confirmed by inspecting the shapes of the optimal fields in Fig. 3. The blue field connecting  $|i\rangle$  and  $|r\rangle$  plays the role of the Stokes pulse and the red field connecting  $|0\rangle$  and  $|i\rangle$  that of the pump pulse in the first half of the time interval. These roles are reversed in the second half. The middle part of the interval, between 20 ns and 50 ns is crucial for obtaining the non-local phase, as can be seen from the significant population of the  $|rr\rangle$  state. The dynamics of the  $|00\rangle$  and the  $|01\rangle$ ,  $|10\rangle$  states are locked. This is due to the fact that we optimize for a non-local phase  $\chi$  in the  $|11\rangle$  state. However, the  $|11\rangle$  state does not couple to the laser fields. The non-local phase, which is given by  $\chi = \phi_{00} - \phi_{01} - \phi_{10} + \phi_{11}$  [22], is thus achieved



**Fig. 2** Minimizing the population in the unstable state  $|i\rangle$ : population dynamics for the sixteen electronic states ( $|11\rangle$  is not shown since the population is equal to one for all times). The radiative lifetime of the states  $|i\rangle$  and  $|r\rangle$  is described by a non-Hermitian Hamiltonian.



**Fig. 3** Optimal shapes of the laser fields and corresponding spectra, employing the constraint to minimize population of  $|i\rangle$ .

by ‘coordinating’ the time evolution of the remaining three two-qubit states which can be controlled by the laser fields.



gate time $T$	gate error $\epsilon$
20ns	0.067
25ns	0.051
30ns	0.001 $\rightarrow$ 0.003
35ns	0.001
40ns	0.001
45ns	0.002
50ns	0.003
60ns	0.003

**Table 2** Optimal gate errors as a function of gate time, neglecting losses from both the intermediate state  $|i\rangle$  and the Rydberg state  $|r\rangle$ . The shortest possible gate time to achieve a reasonable fidelity is then limited by the interaction in the excited state and the motion in the trap. The error increases to  $\rightarrow 0.003$  (at 30 ns) when a lifetime of  $20 \mu\text{s}$  for the Rydberg level is included, consistent with the estimates of Sec. 3.3.

## 2.5 Ignoring spontaneous emission: Rabi flop sequence

If the Rydberg state could be accessed directly, gate error  $\epsilon$  and time  $T$  would be solely determined by the interaction strength in the Rydberg state and the trap frequency [22]. We examine this scenario by ignoring the instability of the intermediate state  $|i\rangle$  and applying the standard control functional, Eq. (6). Table 2 lists the minimal gate error  $\epsilon$  neglecting the spontaneous decay from the intermediate state for a number of gate times  $T$ . Optimization was performed for a non-local phase in the  $|00\rangle$  state. Inspection of Table 2 reveals that the minimum gate operation time is about 30 ns with a gate error of the order of  $10^{-3}$ . This limit is imposed by the interaction strength in the Rydberg state  $|rr\rangle$ . The fact that the gate error increases as  $T$  is enlarged, indicates that excitation of motion in the trap starts to play a role. Including the trapping potential in the calculation for the qubit states during the gate allows motional excitation to be further reduced [21].

The population dynamics of each electronic state induced by the optimal fields shown in Fig. 4 are clearly non-adiabatic. The intermediate state  $|i\rangle$  is significantly populated at intermediate times since the optimization algorithm does not ‘know’ that  $|i\rangle$  corresponds to a loss channel. The population of the Rydberg state in the middle of the time interval is larger in Fig. 4 than in Fig. 2. This explains why a smaller gate duration can be achieved. The optimal pulse shapes and spectra are shown in Fig. 5. The observed sequence of fast switches of both red and blue laser fields pumps population in a ladder-like fashion with a time constant equal to the duration of a  $\pi$ -pulse at the maximally allowed Rabi frequency. Correspondingly, we observe stronger sidebands in the spectra of the optimal pulses (compare Figs. 3 and 5).

In summary, we find minimum gate durations of about 30 ns to 50 ns for a high-fidelity implementation of the Rydberg gate. Shorter gate operation times might be possible by employing higher lying Rydberg states which exhibit a stronger interaction. However, higher states will also be more sensitive to stray fields. While our model includes all relevant degrees of freedom and spontaneous emission from the excited states, noise sources that are inevitably present in any experimental setup need to be analysed in order to gain a full understanding of what fidelities can be achieved in an experiment based on optimized pulse shapes. The influence of noise sources is expected to be particularly detrimental for miniaturized setups such as an atom chip.

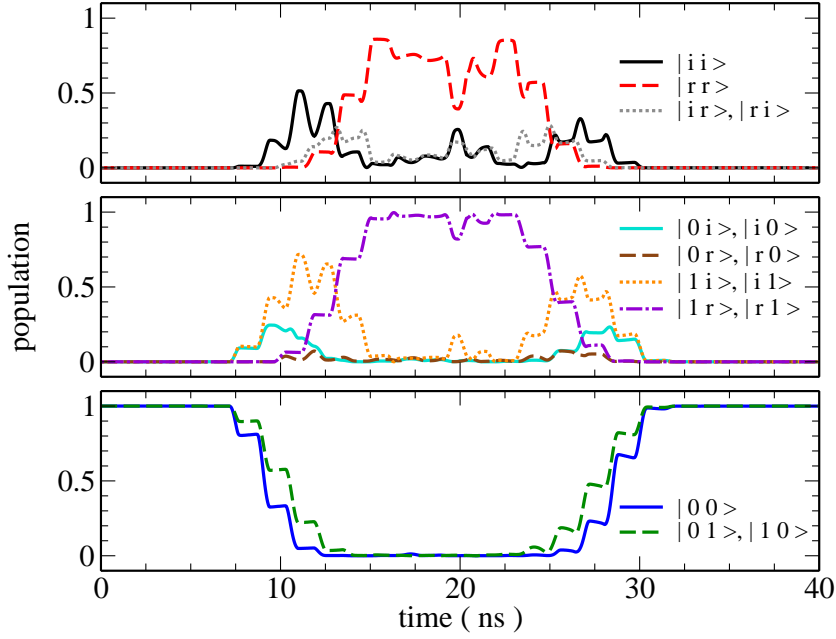


**Fig. 4** Two-photon excitation scheme treating the intermediate state  $|i\rangle$  as stable: population dynamics for the sixteen electronic states. ( $|11\rangle$  is not shown since the population is equal to one for all times.)

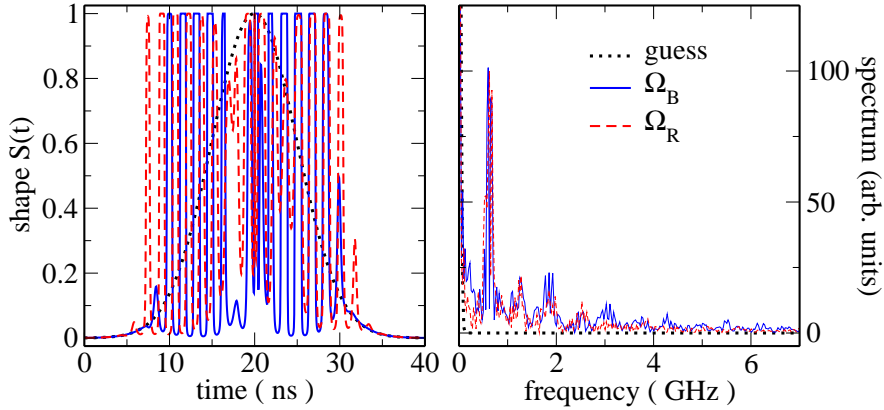


**Fig. 5** Optimal shapes of the laser fields and corresponding spectra, assuming the intermediate state  $|i\rangle$  to be stable.

### 3 Influence of noise

The hyperfine ground-state levels  $|0\rangle$ ,  $|1\rangle$ , as defined in Sec. 2.1, provide a qubit robust with respect to noise, as has been discussed elsewhere [23, 24, 25] and demonstrated experimentally [34]. We therefore focus here on the specific sensitivity of the Rydberg state  $|r\rangle$  to static and fluctuating fields typical for an atom chip environment. Since the Rydberg levels are populated only over the duration of the

laser pulse (some 10 ns) and their angular momenta are relatively small ( $j \leq 5/2$ ), we do not have to consider magnetic field noise that takes effect only on a time scale of 100 ms or longer [25].

### 3.1 Surface impurities: DC Stark shifts

Previous work has shown that the surfaces of atom chips get contaminated with adsorbed atoms that lead to randomly placed charges or dipoles [35]. As a typical scenario, consider an alkali atom on a metal that gives off its electron into the surface so that an upright dipole moment remains. At a distance  $z \approx 10 \mu\text{m}$  above it, this single impurity creates a tiny electric field of the order of

$$E_{\text{imp}}(z) \sim \frac{2ea_B}{4\pi\epsilon_0 z^3} = 0.15 \frac{\text{mV}}{\text{m}}, \quad (10)$$

where  $a_B$  is the Bohr radius. But if  $10^4$  adatoms are distributed over an area of  $(10 \mu\text{m})^2$ , (corresponding to an average distance  $\sim 100 \text{ nm}$ , i.e., much less than a monolayer), their electric fields roughly add up to  $\mathcal{O}(1 \text{ V/m})$ . The corresponding Stark-Hamiltonian,

$$H_S = -\hat{\boldsymbol{\mu}} \cdot \mathbf{E}_{\text{imp}}(z), \quad (11)$$

has matrix elements of the order  $ea_B n^2 E_{\text{imp}}(z) \approx 6.6 \text{ MHz}$  for  $n = 58$ , just one order of magnitude below the Rydberg interaction Hamiltonian (3). The experiments of Ref. [35] have actually detected electric fields up to 1 kV/m at a distance of about  $10 \mu\text{m}$ . On an insulating surface, charges can be trapped and the fields would even be stronger. Note that the threshold for field ionization is of the order of 5 kV/m for the  $n = 58$  level [36].

The Rydberg level considered here,  $|r\rangle = |nd_{3/2}\rangle$  ( $n = 58$ ), is actually “protected” from a linear Stark shift because its quantum defect ( $\delta_d \approx 1.34$ ) lifts the degeneracy with the opposite parity states  $|np, f, \dots\rangle$ , by an energy splitting of the order of  $\Delta_n = 1/n^3 \text{ a.u.} \approx 1.125 \text{ cm}^{-1} = 33.7 \text{ GHz}$  (see Fig. 6 (left)). For this reason, the Stark shift is quadratic in the field and inversely proportional to the detuning ( $< \Delta_n$ ) from the nearest level with opposite parity. The nearest levels 57f and 59p give quadratic Stark shifts that partially cancel each other, leaving a polarizability for 58d of the order of  $50 \text{ kHz(V/m)}^{-2}$ . The 56f state shows a much larger polarizability because the hydrogen manifold  $56\text{H} = 56\text{g, h, } \dots$  is only about  $0.02 \text{ cm}^{-1}$  ( $\approx 600 \text{ MHz}$ ) away (Fig. 6 (right)) and its influence is not cancelled by another level. We estimate a quadratic Stark effect of the order of  $2 \dots 3 \text{ MHz(V/m)}^{-2}$ .

This means that fields above 1 V/m start to detune the so-called Förster resonance between the two-atom states  $|58d_{3/2} 58d_{3/2}\rangle$  and  $|56f_{5/2} 60p_{1/2}\rangle$  whose energy mismatch is only  $7 \text{ MHz} \approx 2.3 \cdot 10^{-4} \text{ cm}^{-1}$  (see Fig. 6 (right) and Refs. [37, 26]). One then loses the strong  $1/r^3$  scaling of the Rydberg interaction that turns into the weaker  $1/r^6$  van der Waals scaling. In addition, at the level of 10 V/m, the linear DC Stark shift of the hydrogen-like state manifold  $|56\text{H}\rangle$  exceeds  $\approx 600 \text{ MHz}$ . By an avoided crossing, the state  $|56f_{5/2}\rangle$  is then pushed down, and the Förster resonance is detuned.

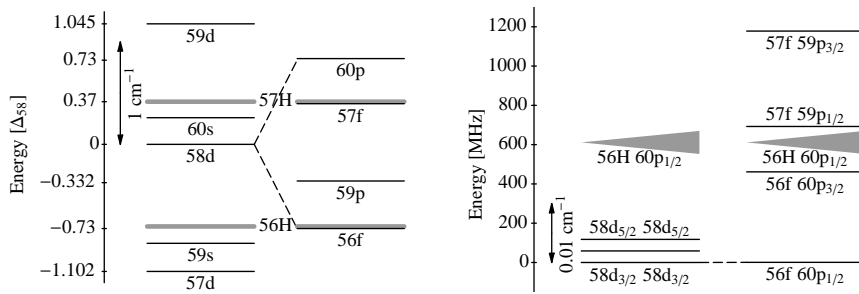


**Fig. 6** (left) Energy levels near the Rydberg state  $|r\rangle = |58d_{3/2}\rangle$ . The strong Rydberg interaction arises from the near degeneracy of  $|rr\rangle$  with the two-atom level  $56f_{5/2} 60p_{1/2}$  (“Förster resonance” [37], dashed lines). The fine structure is not resolved on the scale  $\Delta_{58} = 1/58^3$  a.u. = 33.7 GHz. The thick gray lines (label  $nH$ ) give the hydrogen-like state manifold beyond the  $nf$  states (angular momenta  $l > 3$ ). The left and right columns show even and odd orbital angular momentum states.

(right) Energy levels of the two-atom system. The levels in the Förster resonance are connected by the dashed line (detuning  $\approx 7$  MHz [26]). At a distance  $r_0 \approx 4 \mu\text{m}$ , the two levels hybridize and split by  $\approx 50$  MHz, as described by the two-atom Hamiltonian (3). Note the difference in scale: the fine structure of the p and d levels is resolved (but not for the f levels). A quantum defect of order  $10^{-2}$  splits off the level  $56f$  from the hydrogen-like manifold  $56H = 56g, h, \dots$ . The gray triangles illustrate the linear Stark splitting of  $56H$  in a weak static electric field between 0 and 1 V/m (shifts up to  $\pm 60$  MHz). At slightly higher fields, also the levels  $57f 59p_{1/2}$  and  $56f 60p_{3/2}$  would be pushed away (avoided crossings). The quadratic Stark shift of the other levels is not visible on this scale.

The energy levels are calculated from quantum defect data collected in Refs. [38, 39]. A precise localization of the Förster resonance (not attempted here) would require knowledge of the quantum defects at the  $10^{-4}$  level.

### 3.2 Fluctuating fields: dephasing

The one- and two-atom Rydberg states that we are considering do not feature a permanent electric dipole moment. This is due to the quantum defects that split them off the hydrogen-like manifolds of higher angular momentum states ( $l > 3$ ). In weak fields, their Stark effect is therefore quadratic. We consider here the beating between a fluctuating field and a static impurity field  $E_{\text{imp}}(z)$  at the level of 1 V/m, small enough not to perturb the dipole-dipole interactions, see previous section. The mixing of states with opposite parity is linear in the impurity field and translates into a dipole moment of the order of  $d_R = \alpha_R E_{\text{imp}}(z)$  where  $\alpha_R$  is the quasi-static polarizability. For the level  $58d_{3/2}$ , the contributions to nearby levels above and below partially cancel, leading to the relatively small value  $|d_R| \sim 4 ea_B$ . The level  $56f_{5/2}$  is much more polarizable, as found above, and  $d_R \sim 200 ea_B$ . Note that this is still much smaller than expected from the average size of a Rydberg atom ( $\approx a_B n^2$ ). The fluctuating phase shift due to the Rydberg polarizability  $\alpha_R$  is then given by

$$\Delta\phi(\tau) = - \int_{t_1}^{t_2} dt \frac{\alpha_R}{\hbar} \mathbf{E}_{\text{imp}}(z) \cdot \mathbf{E}_{\text{fluct}}(z, t), \quad (12)$$

where the time integral is evaluated over that part of the pulse that the atom effectively spends in the Rydberg level (see Figs. 2, 4).

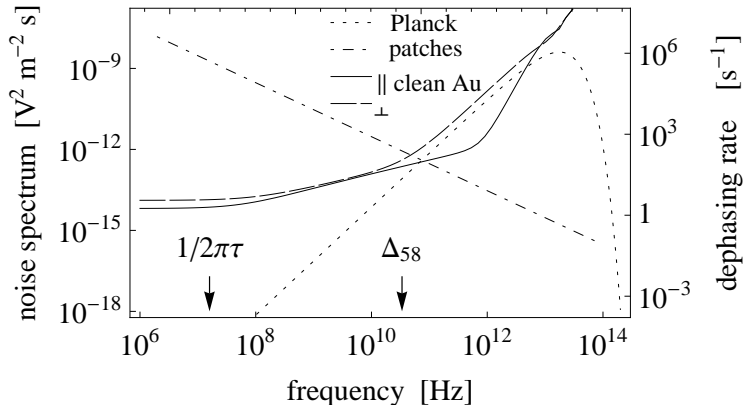


**Fig. 7** Electric field noise spectrum (in  $(\text{V}/\text{m})^2/\text{Hz}$ ) due to patch charge fluctuations (dot-dashed) and due to Johnson-Nyquist noise from a gold half-space (solid and dashed lines). Distance fixed to  $z = 10 \mu\text{m}$ , temperature 300 K. Patch fluctuations are calculated from Ref. [40] and extrapolate ion trap data (in the MHz range), assuming a  $1/\omega$  scaling. The Johnson-Nyquist noise is calculated along the lines of Ref. [41]. It includes blackbody radiation and free-space vacuum fluctuations and changes from a  $\omega^{1/2}$  into a  $\omega^2$  power law near the typical Rydberg transition energy  $\Delta_{58}$  (arrow). Solid (dashed) lines are for fields parallel (perpendicular) to the surface, respectively. The right scale gives the expected dephasing rate for a static dipole moment  $\mathcal{O}(200 ea_B)$  and a white spectrum. The arrow at  $1/2\pi\tau$  marks the Fourier-limited band width for quasi-static noise over an effective interaction time  $\tau = 10 \text{ ns}$ . The contribution of quantum fluctuations was subtracted in the Planck spectrum (dotted curve).

Let us assume an electric field noise spectrum with a scaling

$$S_E(z, \omega) = \frac{S_E(z_0, \omega_0)}{(z/z_0)^4} \left(\frac{\omega_0}{\omega}\right)^\beta \quad (13)$$

that arises from “patch charge” fluctuations, as observed in experiments with miniaturized ion traps [40, 42, 43] (exponent  $\beta \approx 0.7 \dots 1$ ). The  $1/z^4$  scaling actually only holds at heights  $z$  beyond a characteristic length scale for the patch size. This effect is taken into account in the plots shown, using the model of Ref. [40]. The thermal electric fields that originate from the motion of charges in the chip material (Johnson-Nyquist noise) have a lower noise spectrum compared to the patch charge model of Eq. (13) [41, 42, 44], at least in the low-frequency range (up to a few MHz) relevant for dephasing. This is illustrated in Fig. 7 where the two noise spectra (at fixed distance  $10 \mu\text{m}$ ) are plotted vs frequency.

The dephasing of the Rydberg state is now estimated by calculating the variance of the phase shift (12). Provided the interaction time  $\tau = t_2 - t_1$  is large compared to the noise correlation time, the variance increases like

$$\overline{\Delta\phi^2(\tau)} \approx \tau \frac{d_R^2 S_E(z_0, 1/\tau)}{2\hbar^2 (z/z_0)^4} \frac{1}{\cos(\pi\beta/2)\Gamma(2+\beta)}, \quad (14)$$

where the noise spectrum is evaluated at  $\omega = 1/\tau$ , roughly the Fourier-limited bandwidth of the pulse, and  $\Gamma(\cdot)$  is Euler’s gamma function. For room-temperature microscopic ion traps [43, 40, 45, 46], noise levels of  $S_E(75 \mu\text{m}, 1 \text{ MHz}) \sim 10^{-11} (\text{V}/\text{m})^2/\text{Hz}$  and  $\beta \approx 0.7 \dots 0.8$  are typical. Note that a low-frequency cutoff must be applied

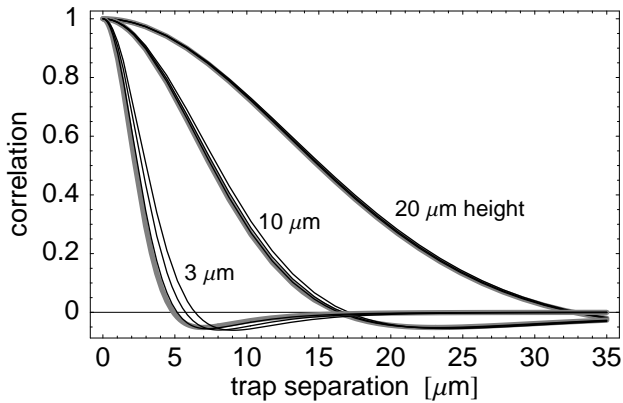


**Fig. 8** Normalized cross-correlation of electric field noise due to patch charge fluctuations, evaluated at three different positions and normalized to the noise spectrum in one trap. If the correlation is weak, the relative phase of the Rydberg state in the two traps is randomized on the same time scale as the common phase. The correlations are calculated by generalizing the model of Ref. [40]. Any group of three curves corresponds to patch correlation lengths 0.5, 1, and 1.5  $\mu\text{m}$ .

for pure  $1/f$  noise. Taking an effective time of  $\tau \approx 20$  ns spent in the Rydberg level, one gets at  $z = 10 \mu\text{m}$  a dephasing rate of

$$D_{\phi}(56f) = \overline{\Delta\phi^2(t)}/\tau = \mathcal{O}(10^6 \text{ s}^{-1}) \quad (15)$$

for the highly polarizable Rydberg state. This affects in particular the two-Rydberg state via its admixture of  $56f\ 60p$  (Fig. 6). For the phase gate, we get a sizable decoherence error  $\epsilon \approx 1 - \langle e^{i\Delta\phi(\tau)} \rangle \approx \frac{1}{2}D_{\phi}\tau \sim 1\%$  from the uncertainty in the two-atom phase  $\phi_{11}$ . We recall that this number scales quadratically with the impurity field, assumed here to be 1 V/m. The other Rydberg levels involved show a much smaller dephasing, in particular  $D_{\phi}(58d) = \mathcal{O}(400 \text{ s}^{-1})$ . This is insignificant over the effective pulse duration  $\tau$ , and therefore the one-atom phases  $\phi_{01}$ ,  $\phi_{10}$  are not compromised.

One may ask the question to what extent the fields seen by the two atoms are correlated. The phase gate misses its target already, of course, if there are fluctuations that are common to both atoms. A differential phase would mix the even and odd states  $|56f_{5/2}\ 60p_{1/2}\rangle \pm |60p_{1/2}\ 56f_{5/2}\rangle$  that are involved in the Förster resonance. This can be quantified from the cross-correlation spectrum of the patch fields,  $S_E(A, B; \omega)$ , where  $A$  and  $B$  are the positions of the two traps. In Fig. 8, we plot the normalized cross-correlation for two atoms at the same distance  $z$  from the chip, but laterally separated by a length  $r_0$ . The two atoms are subject to the same noise (no differential dephasing) if the normalized correlation is unity. One notes that the fields decorrelate on a scale given by the height above the surface. The correlation is still quite strong for the parameters we considered here, i.e. a separation  $r_0 = 4 \mu\text{m}$  and height  $10 \mu\text{m}$ .

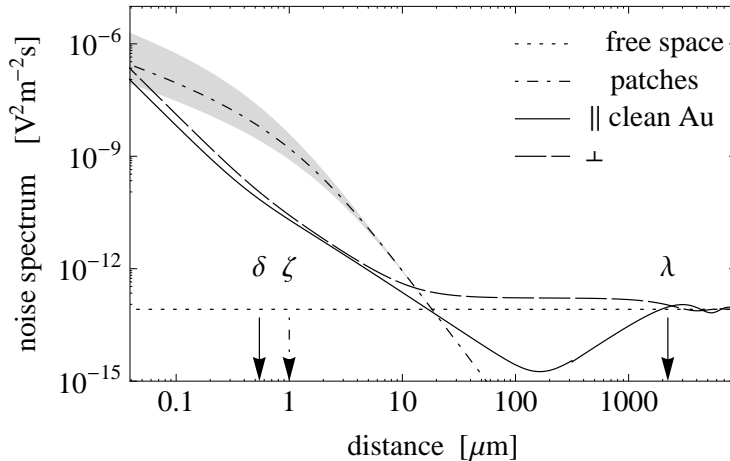


**Fig. 9** Electric field noise spectra (in  $(\text{V}/\text{m})^2/\text{Hz}$ ) vs distance from the chip surface, evaluated at the level splitting  $\Delta_{58}$  typical for Rydberg transitions, and 300 K. The patch charge spectrum is extrapolated to this frequency assuming a  $1/\omega$  scaling; the patch correlation length is in the range  $\zeta = 1 \pm 0.5 \mu\text{m}$  (shaded area). The solid and dashed curves “clean Au” give the noise spectrum of thermal near field radiation, the far field limit is shown by the dotted line. The skin depth  $\delta$  separates two power laws [41], and for  $z \gtrsim \lambda/2$ , the spectrum oscillates due to interference by reflection from the surface. In this limit, a perfect conductor approach yields good agreement. Within the wide plateau between  $10 \mu\text{m}$  and  $1 \text{mm}$ , a dipole perpendicular to the surface ( $\perp$ ) is subject to near field noise about five times as strong as the free space (Planck) level.

### 3.3 Thermal radiation: lifetime and AC Stark shift

The radiative lifetime of an emitter is strongly modified in the vicinity of a macroscopic body, as illustrated by the Purcell effect [47]. In addition, thermal radiation plays a significant role because the Bohr frequencies of Rydberg atoms are low, typically  $\Delta_n \ll k_B T$ . It is well known that this reduces the lifetime and coherence time of trapped particles, even to the level that magnetic dipole transitions become relevant [25]. We estimate here surface-enhanced radiative loss and discuss that despite the large polarizabilities, thermal radiation gives rise to AC Stark shifts that are overall small, leaving only the zero-temperature van der Waals shift. A similar question has been addressed in Refs. [48, 49].

Spontaneous emission in free space is dominated by the decay into the lowest states because of the cubic scaling of the vacuum field spectrum. This leads to a lifetime of the Rydberg state of  $210 \mu\text{s}$  at  $T = 0$  [50] and a decay probability, i.e., gate error, of the order of  $10^{-4}$  given the Rydberg excitation time  $\tau \approx 20 \text{ns}$ . We therefore need to check that this error does not increase significantly in an atom chip environment. The contribution of blackbody radiation reduces the lifetime significantly (absorption and emission), to a total figure of roughly  $90 \mu\text{s}$  for the Rydberg level  $58d$  where the effective quantum number is  $n^* \approx 58 - 1.34$  [50].

The chip surface enhances the mode density of the electromagnetic field [48, 51, 52]. This leads to a different scenario, however, for transitions with large or small Bohr frequencies. For the decay into low states, the resonant wavelengths

are typically in the visible and near UV, small compared to the atom-surface distance. These field modes form a shallow interference pattern due to reflection at the surface, enhancing or suppressing the decay by roughly a factor of 2. Destructive interference can be used to suppress certain decay channels, as suggested in Ref. [53] in an application of the Purcell effect [47].

At smaller Bohr frequencies, thermally stimulated emission and absorption are enhanced much more strongly in the near field. This can be calculated from the approach of Wylie and Sipe [51, 48]. The rate for a transition  $r \rightarrow s$  is given by

$$\gamma_{r \rightarrow s} = \frac{2[1 + \bar{n}(\omega_{rs})]}{\hbar} \sum_{kl} \langle s | \mu_k | r \rangle \langle s | \mu_l | r \rangle^* \mathfrak{Im} [G_{kl}(z; \omega_{rs})], \quad (16)$$

where the Bohr frequency is  $\hbar\omega_{rs} = E_r - E_s$ , and the thermal occupation number  $\bar{n}(\omega_{rs})$  is evaluated at temperature  $T$ . The matrix elements of the dipole operator  $\hat{\mu}$  are written in Cartesian components, and  $G_{kl}$  is the electromagnetic Green tensor at the position  $z$  of the atom. Note that we normalize it such that  $\varepsilon_0 G_{kl}$  has units of inverse volume. This formula also describes the absorption rate of thermal photons ( $\omega_{rs} = -\omega_{sr} < 0$ ) because

$$[1 + \bar{n}(-\omega_{sr})] \mathfrak{Im} [G_{kl}(z; -\omega_{sr})] = \bar{n}(\omega_{sr}) \mathfrak{Im} [G_{kl}(z; \omega_{sr})]. \quad (17)$$

We get the total decay rate  $\gamma_r$  by summing Eq. (16) over the final states  $|s\rangle$ . Fig. 7 can be taken as an illustration of the terms in this sum because the electric field noise spectrum is proportional to  $\mathfrak{Im} [G_{kl}(z; \omega_{rs})] [1 + \bar{n}(\omega_{rs})]$ . The Green tensor is calculated for a gold surface using the formulas of Ref. [51]. The dependence on distance is shown in Fig. 9. Compared to free space (Planck spectrum, dashed line), transitions among Rydberg levels are significantly enhanced at short distances, while the rates oscillate in the opposite limit (distance comparable to the transition wavelength) due to the interference pattern mentioned above. Note the quite strong destructive interference for a transition dipole parallel to the surface (solid curve) which can be understood from the image dipole at a perfectly conducting surface.

The transition rates scale with the electric dipole matrix elements of the Rydberg levels. We note that for a Bohr frequency  $\hbar|\omega_{rs}| \gg \Delta_n$ , the matrix elements are much smaller because a kind of radial selection rule suppresses changes in the principal quantum number by more than a few units (see also Refs. [36, 48]). For a typical final state among adjacent Rydberg levels, for example  $\Delta n^* \lesssim 2$ , we find an enhancement of the transition rate by a factor  $\mathcal{O}(5)$  at  $z = 10 \mu\text{m}$  compared to free space. The corresponding lifetime is reduced from  $\sim 150 \mu\text{s}$  (free space) to  $\sim 30 \mu\text{s}$ , estimating the matrix element by  $ea_B n^{*2}$ . We note that the rate for this generic pair of levels essentially exhausts the thermal decay rate summed over all final states, including photoionization [50]. We therefore expect a total lifetime somewhat below the  $\sim 30 \mu\text{s}$  figure estimated above from a single bound-bound transition. While this is still three orders of magnitude longer than the Rydberg excitation pulse, it may pose a serious challenge to gate errors below the fault tolerance threshold of  $10^{-4}$ . As a preliminary check, we have performed (see Table 2) a calculation of the phase gate error when a finite lifetime  $20 \mu\text{s}$  of the Rydberg level is included: an increase of the order of  $10^{-3}$  is indeed found.

The radiation field also induces a van der Waals–Casimir–Polder shift on the Rydberg levels. We can estimate this in the London limit (transition wavelength



large compared to the atom-surface distance) since the Rydberg spacing  $\Delta_{58}$  corresponds to wavelengths in the centimeter range,

$$V_{\text{vdW}}(z) = -\frac{\langle r | \hat{\mu}_x^2 + \hat{\mu}_y^2 + 2\hat{\mu}_z^2 | r \rangle}{8\pi\epsilon_0(2z)^3}. \quad (18)$$

The expectation value of the squared dipole is of the order of  $\frac{5}{2}(ea_B n^{*2})^2$  (see, e.g., Ref. [54]) and gives a shift  $\approx 1.6$  MHz at  $10 \mu\text{m}$ , consistent with the findings of Ref. [48] where the electric quadrupole contribution is analyzed as well. This is not far from the dipole-dipole interaction (as it must from the scaling), but still small enough not to perturb it. The level shift changes only weakly across the levels shown in Fig. 6 and does not induce significant detunings. Its main impact is therefore to pull the Rydberg atoms towards the chip during the pulse. This effect which excites motional states in the trap, could be compensated for by the exciting laser pulse in a similar way as the momentum exchange between the two Rydberg atoms (see Sec. 2.3).

We finally turn to the question how thermal radiation is shifting the Rydberg levels. This could be significant since even room-temperature blackbody radiation produces a sizable electric field above  $100 \text{ V/m}$ , albeit over a wide frequency range. It has been pointed out that the Casimir–Polder potential is essentially temperature-independent, due to cancellations between different transitions, on the one hand, and virtual and real photon exchange, on the other [49]. This holds provided the typical transition wavelengths are large compared to the atom-surface distance, which is indeed the case for a Rydberg atom. We have checked that this result can be understood in a simple way starting from the dynamical polarizability of a free electron and integrating over the thermal radiation spectrum. For an analysis at zero temperature, see Ref. [55] and references therein. The Planck spectrum gives a free-space level shift, common to all weakly bound Rydberg levels, of the order of  $\alpha_{\text{fs}}(k_B T)^2/(m_e c^2) = \mathcal{O}(2 \text{ kHz})$ , where  $\alpha_{\text{fs}}$  is the fine structure constant and  $m_e c^2$  the electron’s rest energy. This is consistent with the value quoted in Ref. [36]. Near the chip surface, the shift is modified by a factor  $\lambda_T/z$ , where  $\lambda_T = \hbar c/k_B T \approx 7.6 \mu\text{m}$  is Wien’s thermal wavelength. The result is still negligible on the energy scale set by the Rydberg dipole-dipole interaction, and we provide a detailed discussion elsewhere.

## 4 Conclusions

We have used optimal control theory to determine the shortest gate duration for a controlled phase gate based on resonant excitation of neutral rubidium atoms to Rydberg levels that show a long-range dipole-dipole interaction. The parameters were chosen to be similar to those of the experiment reported in Ref. [26], in particular a distance between the atoms of  $4 \mu\text{m}$ , a trapping frequency of  $\omega/2\pi \approx 276 \text{ kHz}$ , and near-resonant two-photon interaction to the Rydberg level via the  $5p_{1/2}$  level. It turns out that in this setting the fidelity of the controlled phase gate is limited to a few percent by the strong decay from the intermediate level, despite suppressing the population of the intermediate level as much as possible. The optimal pulses correspond to STIRAP-like transitions to and from the Rydberg state, i.e. an adiabatic solution to the control problem is found. Neglecting spontaneous decay from

the intermediate level (which would correspond to a different excitation scheme to the Rydberg level), gate errors of the order of  $10^{-3}$  are obtained for  $T = 30$  ns and larger. This lower limit on duration is essentially due to the interaction strength of the two atoms in the Rydberg state. The control pulses induce a sequence of Rabi flops, and the ensuing nuclear dynamics is strongly non-adiabatic. Further reduction of the gate error to values below the fault tolerance threshold of  $10^{-4}$  requires the calculation to include the trapping potential for the qubit states during the gate. Otherwise, the motional state of the atoms at the end of the gate is not well-defined to this precision, and higher lying trap states get excited.

These conclusions hold in a general setting where our parameters for trap separation and frequency are applicable. In order to estimate whether a Rydberg phase gate can be implemented on an atom chip to yield a universal quantum computer in a scalable setting, all relevant noise sources specific to the chip environment need to be considered. To summarize the estimates on sensitivity to noise due to the chip environment, we have found serious issues for Rydberg atoms held at a distance of the order of  $10\ \mu\text{m}$ , due to linear and quadratic Stark shifts. The reason is the contamination by impurity atoms of the chip surface at densities higher than  $100\ \mu\text{m}^{-2}$ , still much less than a monolayer. This would create, above a metallic surface, electric fields exceeding  $\mathcal{O}(1\ \text{V/m})$ , and reduce significantly the strong dipole-dipole interaction between the Rydberg atoms. This slows down the quantum gate, and a sizable dephasing rate arises from the beating between stray fields and fluctuating patch potentials, in particular for the highly polarizable  $56f$  state. Operating the chip at lower temperatures would reduce the patch charge noise [43,45]. The radiative decay of the Rydberg state is also enhanced by nearly an order of magnitude compared to free space at zero temperature: we estimate a lifetime in the  $20 \dots 30\ \mu\text{s}$  range. As it stands, this could provide a fundamental lower limit around  $10^{-3}$  to the gate error. Possible improvements may exploit a Purcell effect to suppress, by destructive interference, radiative transitions for certain orientations of the transition dipole, similar to the suggestion in Ref. [53]. This may be achieved with suitably polarized laser pulses. We therefore estimate that reaching errors below the fault tolerance threshold for a Rydberg phase gate on an atom chip is challenging but possible.

**Acknowledgements** We would like to thank Ron Folman for stimulating this work. Financial support from the Deutsche Forschungsgemeinschaft (Ko 2301/2), the German-Israeli Foundation for Scientific Cooperation (982-192.14/2007), and the European Union (Integrated Project AQUITE) is gratefully acknowledged.

## References

1. P. Zoller, T. Beth, D. Binosi, R. Blatt, H. Briegel, D. Bruss, T. Calarco, J.I. Cirac, D. Deutsch, J. Eisert, A. Ekert, C. Fabre, N. Gisin, P. Grangier, M. Grassl, S. Haroche, A. Imamoglu, A. Karlson, J. Kempe, L. Kouwenhoven, S. Kröll, G. Leuchs, M. Lewenstein, D. Loss, N. Lütkenhaus, S. Massar, J.E. Mooij, M.B. Plenio, E. Polzik, S. Popescu, G. Rempe, A. Sergienko, D. Suter, J. Twamley, G. Wendin, R. Werner, A. Winter, J. Wrachtrup, A. Zeilinger, *Eur. Phys. J. D* **36**(2), 203 (2005). DOI 10.1140/epjd/e2005-00251-1
2. M. Nielsen, I.L. Chuang, *Quantum Computation and Quantum Information* (Cambridge University Press, 2000)
3. G.K. Brennen, C.M. Caves, P.S. Jessen, I.H. Deutsch, *Phys. Rev. Lett.* **82**(5), 1060 (1999)

4. D. Jaksch, H.J. Briegel, J.I. Cirac, C.W. Gardiner, P. Zoller, *Phys. Rev. Lett.* **82**(9), 1975 (1999). DOI 10.1103/PhysRevLett.82.1975
5. T. Calarco, E.A. Hinds, D. Jaksch, J. Schmiedmayer, J.I. Cirac, P. Zoller, *Phys. Rev. A* **61**, 022304 (2000)
6. D. Jaksch, J.I. Cirac, P. Zoller, S.L. Rolston, R. Côté, M.D. Lukin, *Phys. Rev. Lett.* **85**(10), 2208 (2000). DOI 10.1103/PhysRevLett.85.2208
7. F.B.J. Buchkremer, R. Dumke, M. Volk, T. Mütter, G. Birkl, W. Ertmer, *Las. Phys.* **12**(4), 736 (2002). URL [http://www.maik.ru/contents/lasphys/lasphys4\\_2v12cont.htm](http://www.maik.ru/contents/lasphys/lasphys4_2v12cont.htm)
8. A.S. Sørensen, C.H. van der Wal, L.I. Childress, M.D. Lukin, *Phys. Rev. Lett.* **92**, 063601 (2004)
9. M.A. Cirone, A. Negretti, T. Calarco, P. Krüger, J. Schmiedmayer, *Eur. Phys. J. D* **35**(1), 165 (2005). DOI 10.1140/epjd/e2005-00175-8
10. P. Treutlein, T.W. Hänsch, J. Reichel, A. Negretti, M.A. Cirone, T. Calarco, *Phys. Rev. A* **74**, 022312 (2006)
11. M. Müller, I. Lesanovsky, H. Weimer, H.P. Buchler, P. Zoller, *Phys. Rev. Lett.* **102**, 170502 (2009). DOI 10.1103/PhysRevLett.102.170502
12. J. Somló, V.A. Kazakov, D.J. Tannor, *Chem. Phys.* **172**, 85 (1993)
13. W. Zhu, J. Botina, H. Rabitz, *J. Chem. Phys.* **108**(5), 1953 (1998)
14. J.P. Palao, R. Kosloff, *Phys. Rev. Lett.* **89**, 188301 (2002)
15. C.M. Tesch, R. de Vivie-Riedle, *Phys. Rev. Lett.* **89**, 157901 (2002). DOI 10.1103/PhysRevLett.89.157901
16. J.P. Palao, R. Kosloff, *Phys. Rev. A* **68**, 062308 (2003). DOI 10.1103/PhysRevA.68.062308
17. T. Caneva, M. Murphy, T. Calarco, R. Fazio, S. Montangero, V. Giovannetti, G.E. Santoro, *Phys. Rev. Lett.* **103**, 240501 (2009). DOI 10.1103/PhysRevLett.103.240501
18. L. Isenhower, E. Urban, X.L. Zhang, A.T. Gill, T. Henage, T.A. Johnson, T.G. Walker, M. Saffman, *Phys. Rev. Lett.* **104**, 010503 (2010). DOI 10.1103/PhysRevLett.104.010503
19. T. Wilk, A. Gaëtan, C. Evellin, J. Wolters, Y. Miroshnychenko, P. Grangier, A. Browaeys, *Phys. Rev. Lett.* **104**, 010502 (2010). DOI 10.1103/PhysRevLett.104.010502
20. M. Saffman, T.G. Walker, K. Mølmer, *Rev. Mod. Phys.* **82**(3), 2313 (2010). DOI 10.1103/RevModPhys.82.2313
21. M.M. Müller, D.M. Reich, M. Murphy, H. Yuan, J. Vala, K.B. Whaley, T. Calarco, C.P. Koch, Getting the best two-qubit gate for a real physical system (2011). arXiv:1104.2337
22. M.H. Goerz, T. Calarco, C.P. Koch, The Quantum Speed Limit of Optimal Controlled Phasegates for Trapped Neutral Atoms (2011). arXiv:1103.6050
23. R. Folman, P. Krüger, J. Schmiedmayer, J.H. Denschlag, C. Henkel, *Adv. At. Mol. Opt. Phys.* **48**, 263 (2002)
24. J. Fortágh, C. Zimmermann, *Rev. Mod. Phys.* **79**(1), 235 (2007)
25. J. Reichel, V. Vuletić (eds.), *Atom Chips* (Wiley-VCH, 2011)
26. A. Gaëtan, Y. Miroshnychenko, T. Wilk, A. Chotia, M. Vitaev, D. Comparat, P. Pillet, A. Browaeys, P. Grangier, *Nature Phys.* **5**, 115 (2009). DOI 10.1038/nphys1183
27. R. Kosloff, *Annu. Rev. Phys. Chem.* **45**, 145 (1994)
28. I. Lesanovsky, P. Schmelcher, *Eur. Phys. J. D* **35**(1), 31 (2005). DOI 10.1140/epjd/e2005-00062-4
29. J. Bill, M.I. Trappe, I. Lesanovsky, P. Schmelcher, *Phys. Rev. A* **73**, 053609 (2006). URL <http://link.aps.org/abstract/PRA/v73/e053609>
30. A. Bartana, R. Kosloff, D.J. Tannor, *J. Chem. Phys.* **106**(4), 1435 (1997)
31. Y. Ohtsuki, W. Zhu, H. Rabitz, *J. Chem. Phys.* **110**(20), 9825 (1999). DOI 10.1063/1.478036
32. J.P. Palao, R. Kosloff, C.P. Koch, *Phys. Rev. A* **77**, 063412 (2008). DOI 10.1103/PhysRevA.77.063412
33. M. Ndong, H. Tal-Ezer, R. Kosloff, C.P. Koch, *J. Chem. Phys.* **130**, 124108 (2009). DOI 10.1063/1.3098940
34. P. Treutlein, P. Hommelhoff, T. Steinmetz, T.W. Hänsch, J. Reichel, *Phys. Rev. Lett.* **92**, 203005 (2004). Erratum *Phys. Rev. Lett.* **93**, 219904(E) (2004)
35. J.M. McGuirk, D.M. Harber, J.M. Obrecht, E.A. Cornell, *Phys. Rev. A* **69**, 062905 (2004)
36. T.F. Gallagher, *Rep. Prog. Phys.* **51**(2), 143 (1988). URL <http://stacks.iop.org/0034-4885/51/143>
37. T.G. Walker, M. Saffman, *J. Phys. B* **38**(2), S309 (2005). URL <http://stacks.iop.org/0953-4075/38/i=2/a=022>
38. C.J. Lorenzen, K. Niemax, *Phys. Scr.* **27**, 300 (1983)
39. W. Li, I. Mourachko, M. Noel, T. Gallagher, *Phys. Rev. A* **67**, 052502 (2003)

40. R. Dubessy, T. Coudreau, L. Guidoni, *Phys. Rev. A* **80**, 031402(R) (2009)
41. C. Henkel, M. Wilkens, *Europhys. Lett.* **47**, 414 (1999)
42. Q.A. Turchette, D. Kielpinski, B.E. King, D. Leibfried, D.M. Meekhof, C.J. Myatt, M.A. Rowe, C.A. Sackett, C.S. Wood, W.M. Itano, C. Monroe, D.J. Wineland, *Phys. Rev. A* **61**, 063418 (2000)
43. J. Labaziewicz, Y. Ge, D.R. Leibbrandt, S.X. Wang, R. Shewmon, I.L. Chuang, *Phys. Rev. Lett.* **101**, 180602 (2008)
44. D. Leibbrandt, B. Yurke, R. Slusher, *Quantum Inf. Comput.* **7**(1-2), 52 (2007)
45. L. Deslauriers, S. Olmschenk, D. Stick, W.K. Hensinger, J. Sterk, C. Monroe, *Phys. Rev. Lett.* **97**, 103007 (2006)
46. R.J. Epstein, S. Seidelin, D. Leibfried, J.H. Wesenberg, J.J. Bollinger, J.M. Amini, R.B. Blakestad, J. Britton, J.P. Home, W.M. Itano, J.D. Jost, E. Knill, C. Langer, R. Ozeri, N. Shiga, D.J. Wineland, *Phys. Rev. A* **76**, 033411 (2007)
47. E.M. Purcell, *Phys. Rev.* **69**, 681 (1946)
48. J.A. Crosse, S.Å. Ellingsen, K. Clements, S.Y. Buhmann, S. Scheel, *Phys. Rev. A* **82**, 010901(R) (2010). Erratum *Phys. Rev. A* **82**, 029902 (2010)
49. S.A. Ellingsen, S.Y. Buhmann, S. Scheel, *Phys. Rev. Lett.* **104**, 223003 (2010)
50. C.E. Theodosiou, *Phys. Rev. A* **30**(6), 2881 (1984)
51. J.M. Wylie, J.E. Sipe, *Phys. Rev. A* **30**(3), 1185 (1984)
52. H. Failache, S. Saltiel, A. Fischer, D. Bloch, M. Ducloy, *Phys. Rev. Lett.* **88**, 243603 (2002)
53. P. Hyafil, J. Mozley, A. Perrin, J. Tailleur, G. Nogues, M. Brune, J.M. Raimond, S. Haroche, *Phys. Rev. Lett.* **93**, 103001 (2004)
54. J.Y. Courtois, J.M. Courty, J.C. Mertz, *Phys. Rev. A* **53**, 1862 (1996)
55. C. Eberlein, D. Robaschik, *Phys. Rev. Lett.* **92**, 233602 (2004)